XL CILAMCE
IBERO-LATIN AMERICAN CONGRESS ON COMPUTATIONAL METHODS IN ENGINEERING
NOVEMBER 11-14, 2019
Praiamar Natal Hotel & Convention
Natal, RN-BRAZIL

LATERAL THRUSTS AND SETTLEMENTS ON A GRANULAR SOIL RETAINED BY A SEMI-INTEGRAL ABUTMENT UNDERGOING CYCLIC LATERAL DISPLACEMENTS WITH DIFFERENT AMPLITUDES

Pedro H. dos S. Silva
Yuri D. J. Costa
eng.phsilva@outlook.com
ydjcosta@ct.ufrn.br
Federal University of Rio Grande do Norte
University Campus, 59072-970, Rio Grande do Norte, Brazil
Jorge G. Zornberg
zornberg@mail.utexas.edu
The University of Texas at Austin
301 E. Dean Keeton, 78712, Texas, The United States of American
Carina M. L. Costa
carina@ct.ufrn.br
Federal University of Rio Grande do Norte
University Campus, 59072-970, Rio Grande do Norte, Brazil

Abstract. Semi-integral abutment bridges are constructed without thermal expansion joints and the superstructure-abutment system is not integrally connected to the substructure. In view of this peculiar characteristics, the abutment undergoes combined movements of translation and rotation due to expansion and contraction of the superstructure caused by temperature variations. Such behavior can increase of lateral thrusts and vertical displacements in the soil close to the abutment. Therefore, this work analyzed lateral thrusts and settlements on a granular soil retained by a semi-integral abutment undergoing cyclic lateral displacements with different amplitudes. A finite element model was developed and calibrated based on field data collected from an instrumented and monitored semi-integral abutment. The soil stress-strain behavior was represented by a hyperbolic constitutive model and the abutment lateral displacements were given by prescribed horizontal displacements. Predictions with the elaborated numerical model were found to produce a good match with the field data. After validation, numerical simulations with displacement amplitudes of ± 5 mm and ± 10 mm were carried out. The passive lateral thrust increased with the lateral displacement amplitude, while the active lateral thrust remained virtually the same in both amplitudes. The settlements, heaves and the disturbance zone within the backfill soil behind the abutment increased with the lateral displacement amplitude.

Keywords: Semi-integral abutment, Numerical simulation, Lateral thrust, Settlement, Heave

1 Introduction

According to Husain and Bagnariol [1], semi-integral abutment bridges (SIABs) are structural systems of single or multiple spans, normally supported by rigid foundations, built without thermal expansion joints but with bearing pads at the abutments. In this case, there is a structural connection only between the superstructure and abutment, resulting in a continuous system not integrally connected to the substructure. Mistry [2] asserts that the absence of thermal expansion joints reduces the bridge susceptibility to problems related to improperly functioning joints due to corrosion that allow attacks of chemical agents on the other bridge elements. Therefore, in consonance with Maruri and Petro [3], the main advantage of using SIABs is the reduction of construction and maintenance costs related to the absence of thermal expansion joints since these devices require adequate and frequent maintenance programs due to their low durability compared to other bridge components.

In view of the peculiar characteristic of SIABs, Ng et al. [4] affirms that expansion and contraction horizontal movements of the superstructure, accumulated over the entire bridge span, are integrally transferred to the abutment and, consequently, to the soil retained behind it. Such behavior favors the increase of lateral earth pressures and soil vertical displacements behind the abutment, resulting in a complex soil-structure interaction mechanism associated with the cyclic horizontal displacement of the superstructure, as reported by Lock [5].

Civjan et al. [6] asserts that the soil response under cyclic movements needs to be defined for typical backfill materials since it depends on load history and rate. Lutenegger et al. [7], Franco [8], Breña et al. [9] and Hasiotis and Xiong [10] have observed a tendency to increase lateral earth pressures next to the abutment for long-span bridges while no increase has been observed for short-span bridges. In relation to soil vertical displacements, Tatsouka et al. [11], Munoz et al. [12], Argyroudis et al. [13] and Saghebfar, et al. [14] have indicated a tendency of increasing downward vertical displacements (settlements) near the abutment, and sometimes including upward vertical displacements (heaves) at a certain distance from the abutment.

Ng et al. [4] carried out centrifuge tests to investigate the performance of an integral bridge abutment. The tests were instrumented to monitor and record the geotechnical response of the backfill behind the abutment undergoing controlled cyclic lateral displacements. Cyclic lateral displacement values were chosen to simulate serviceability, ultimate and extreme conditions of a typical abutment retaining a dry granular material. The results showed an increase of the passive lateral earth pressure coefficient and the settlement with the displacement amplitude and the number of cycles while no increase was observed for the active lateral earth pressure coefficient.

Huntley and Valsangkar [15] presented and discussed field data of lateral earth pressure from an instrumented integral abutment bridge whose abutment retains a backfill composed by a free-draining material. The study analyzed the data of seasonal lateral earth pressure variation throughout a period of three years and observed a slight tendency of increase of the lateral earth pressure with seasonal temperature cycles during the monitored period. Furthermore, the study also identified the need of a greater monitoring period to better understand the actual behavior of seasonal lateral earth pressure variations behind the abutment.

Caristo et al. [16] performed numerical simulations using finite elements to analyze the complex soil-structure interaction between an integral abutment and a compacted sand backfill. The study analyzed the lateral earth pressures and the soil vertical displacements behind the abutment by applying 120 cycles of prescribed horizontal displacement ranging from -27 mm to + 27 mm to simulate the seasonal effects which the bridge would be exposed to over its design life. The results showed that the lateral earth pressures built up quickly during the first 30 cycles before reaching a tendency of stabilization after the 30^{th} cycle. Moreover, settlements were observed behind the abutment with heaves occurring at greater distances from the abutment.

Experience with the use of SIABs is still restricted to some countries mainly due to several uncertainties associated to the complex soil-structure interaction mechanism and the long-term behavior. Understanding the soil behavior behind the abutment under cyclic lateral displacements to

address properly the complex soil-structure interaction mechanisms involved in SIABs is essential. Therefore, the purpose of the present investigation is to assess the effects of cyclic lateral displacement amplitudes on lateral thrusts and settlements on a granular soil retained by a semi-integral abutment through numerical simulations.

2 Methodology

Numerical simulations of a semi-integral abutment were carried out using the software Plaxis 2D 2016, which uses the finite element method. Plane-strain conditions were used in a two-dimensional finite element analysis. A numerical model was developed and calibrated based on the field data from the west abutment of a semi-integral abutment bridge instrumented and monitored by Walter [17]. The model boundaries extended to a width of 40 m in the horizontal direction and a depth of 20 m in the vertical direction. These dimensions were chosen based on the information of Knappett et al. [18] and Rawat and Gupta [19] and were assumed to be enough to exclude boundary effects. The abutment-cap system was assumed as a reinforced concrete structure supported by a driven steel sheet pile foundation, as reported by Walter [17]. Figure 1 shows the geometry adopted for the abutment-cap system.

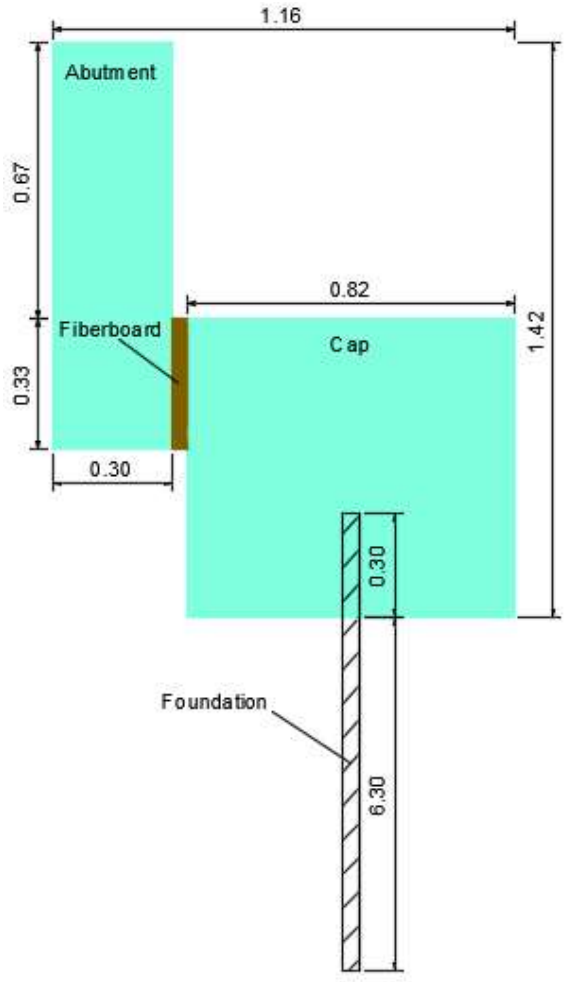

Figure 1. Geometry of the abutment-cap system (dimension in m).

According to Walter [17], the site subsoil at the west abutment can be categorized by a silty sand layer over a sandy clay layer with a gravel spaced at 1V:3H (where V is vertical, and H is horizontal) increments along the width of the abutment. Therefore, a 6.50-m silty sand layer over a 13.5-m sandy clay layer and a gravel spaced at 1V:3H increments next to the abutment were adopted in the

numerical model. The finite element mesh used in the numerical simulations was a very fine mesh composed by 15-node triangular elements and with automatic refinement on the interfaces of the soil-structure interaction. Figure 2 shows the finite element mesh used in the numerical simulations.

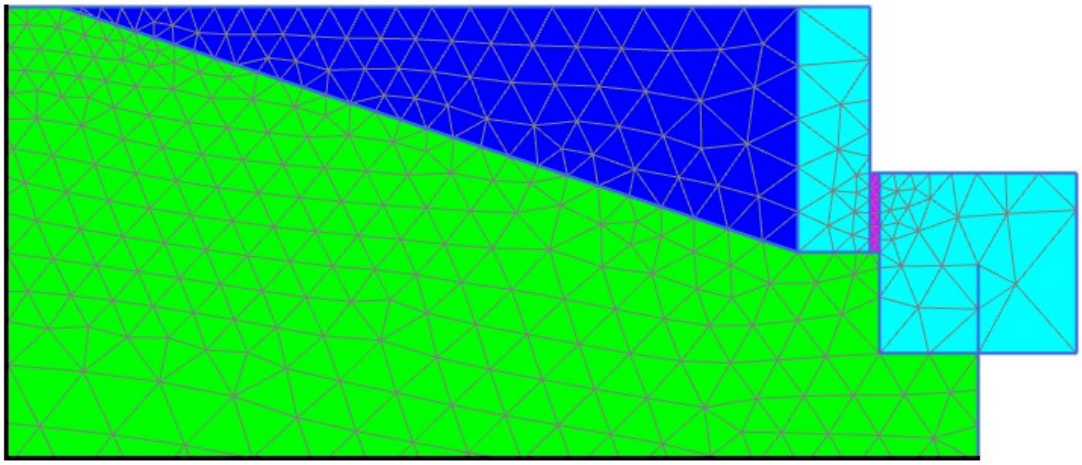

Figure 2. Finite element mesh.

The behavior of the soil materials was represented by the Hardening Soil hyperbolic constitutive model. According to Khanal [20], this constitutive model is based on the Plasticity Theory and was developed to simulate sandy and clayey soils. The structural concrete and the fiberboard were modeled with the linear elastic constitutive model. The sheet piles of the foundation were modeled using plate elements and the behavior was assumed as linear elastic. Soil-structure interaction was considered by using interface elements with strength reduction factors (R_{inter}) equal to 0.5 for soil-steel interface, and 0.7 for soil-concrete interface. A virtual thickness factor of 0.1 was also applied to the interface boundaries.

The parameters of the clayey soil adopted in the numerical model were unsaturated unit weight (γ_{unsat}) equal to 19 kN/m³, saturated unit weight (γ_{sat}) equal to 22 kN/m³, secant stiffness in standard drained triaxial test (E_{50}^{ref}) equal to 60 MPa, tangent stiffness for primary oedometer loading (E_{oed}^{ref}) equal to 60 MPa, unloading/loading stiffness (E_{ur}^{ref}) equal to 180 MPa and undrained shear strength at reference level ($S_{u,ref}$) equal to 210 kPa. The parameters of the sandy soil adopted in the numerical model were γ_{unsat} equal to 17 kN/m³, γ_{sat} equal to 20 kN/m³, E_{50}^{ref} equal to 40 MPa, E_{oed}^{ref} equal to 40 MPa, E_{ur}^{ref} equal to 120 MPa, effective cohesion (c'_{ref}) equal to 15 kPa and effective friction angle (ø') equal to 31.5°. The gravel parameters adopted in the numerical model were γ_{unsat} equal to 20 kN/m³, γ_{sat} equal to 23 kN/m³, E_{50}^{ref} equal to 32 MPa, E_{oed}^{ref} equal to 32 MPa, E_{ur}^{ref} equal to 96 MPa, c'_{ref} equal to 1 kPa and ø' equal to 40°. These soil parameters were estimated based on information from Poulos and Davis [21], Stroud and Butler [22], Mesri [23], Kulhawy and Maine [24] and Tomlinson [25] for typical soil types.

The concrete parameters adopted in the numerical model were unit weight (γ) equal to 25 kN/m³, Young's modulus (E) equal to 30 GPa and Poisson's ratio (ν) equal to 0.2. The fiberboard parameters adopted in the numerical model were γ equal to 10 kN/m³, E equal to 4 GPa and ν equal to 0.2. The plate parameters adopted in the numerical model were weight (w) equal to 1.182 kN/m/m, normal stiffness (EA) equal to 3.163×10^6 kN/m, flexural rigidity (EI) equal to 73.27×10^3 and ν equal to 0.3.

Prescribed horizontal displacements (δh) were used to represent the cyclic lateral displacements at the abutment. According to Karalar and Dicleli [26] and Murphy and Yarnold [27], the lateral displacements (ΔL) at the abutment can be estimated by Eq. (1)

$$\Delta L = \frac{\alpha L \Delta T}{2} \tag{1}$$

where α is the coefficient of thermal expansion, L is the length and ΔT is the temperature variation. The α value assumed for the concrete was 10.8 x 10-6/°C and is in the range recommended by AASHTO [28] in the absence of laboratory tests or more precise data. The ΔT and L values were obtained from Walter [17]. Figure 3 shows the estimated prescribed horizontal displacements

considering the first 100 days of monitoring.

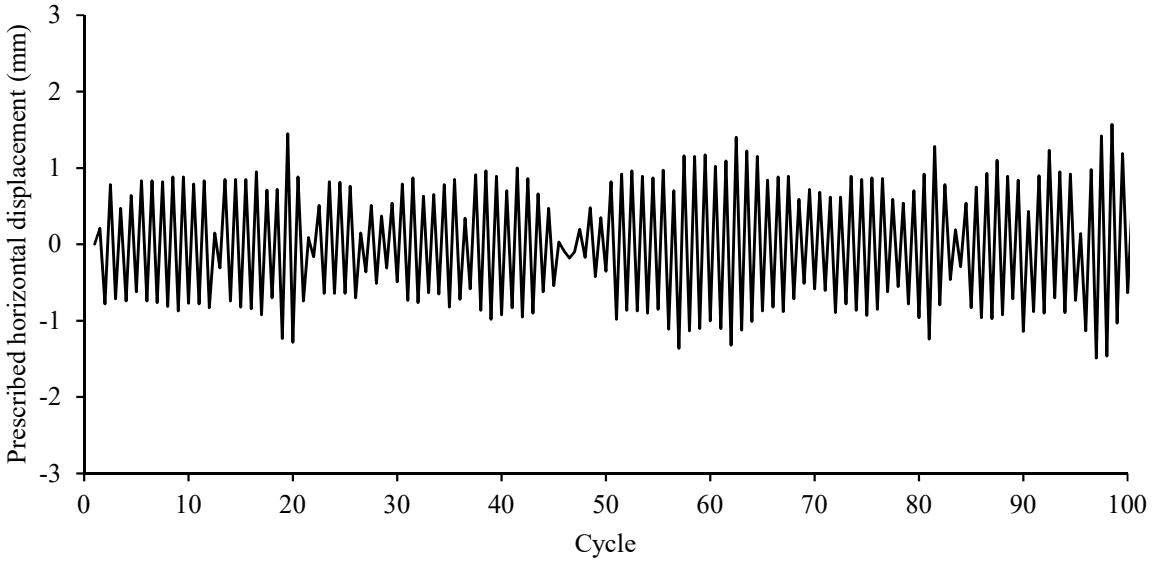

Figure 3. Estimated prescribed displacement representing the lateral movements of the abutment.

The application point of the prescribed horizontal displacement was defined at the top of the backfill-abutment interface since this is the major section of interest. Assumption of larger lateral displacements at the top of the backfill-abutment interface was considered a realistic approach, since, as observed by Rodriguez et al. [29], most changes in temperature take place within the upper third of the bridge superstructure.

3 Results and discussion

Figure 4 compares the maximum and minimum values of horizontal stresses measured with the corresponding numerical predictions.

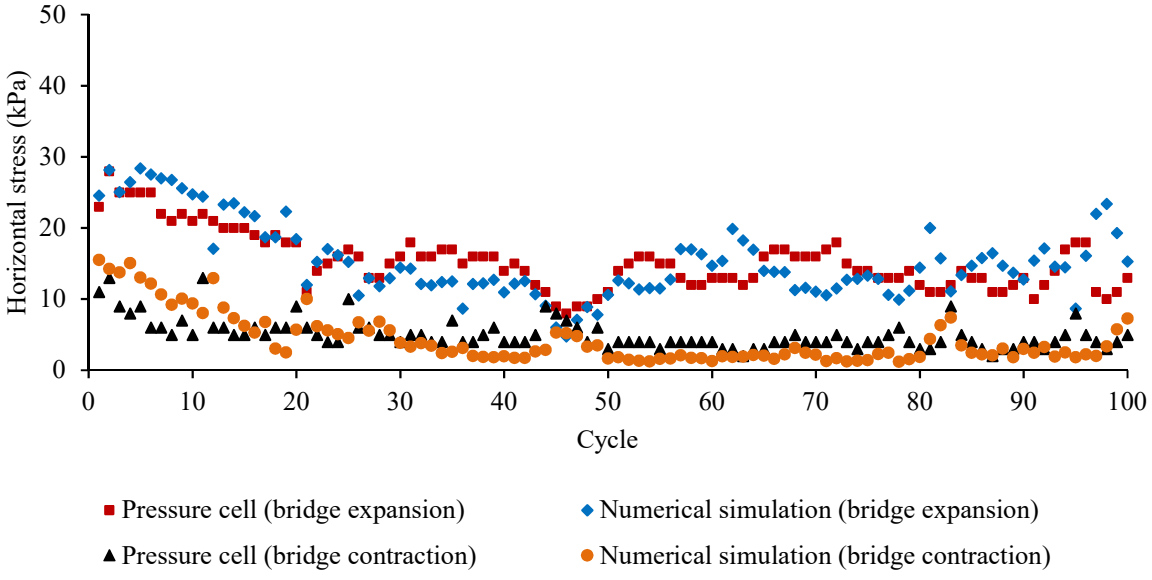

Figure 4. Comparison between measured data and numerical results.

The numerical stress values represent the average of stresses in six stress points along the

abutment height, as to coincide with the same position of installation of the pressure cells in the backfill. It is possible to observe that, in general, prediction with the numerical model produced a good match with field data. Therefore, the numerical model validation can be considered satisfactory, given the many variables and inherent imprecisions involved in the whole process.

Figures 5 and 6 show the calculated lateral thrust on the abutment during expansion (passive lateral thrust) and contraction (active lateral thrust) of the bridge, respectively. Variations of the lateral thrust are associated with the cyclic changes of the imposed horizontal displacements due to temperature fluctuations.

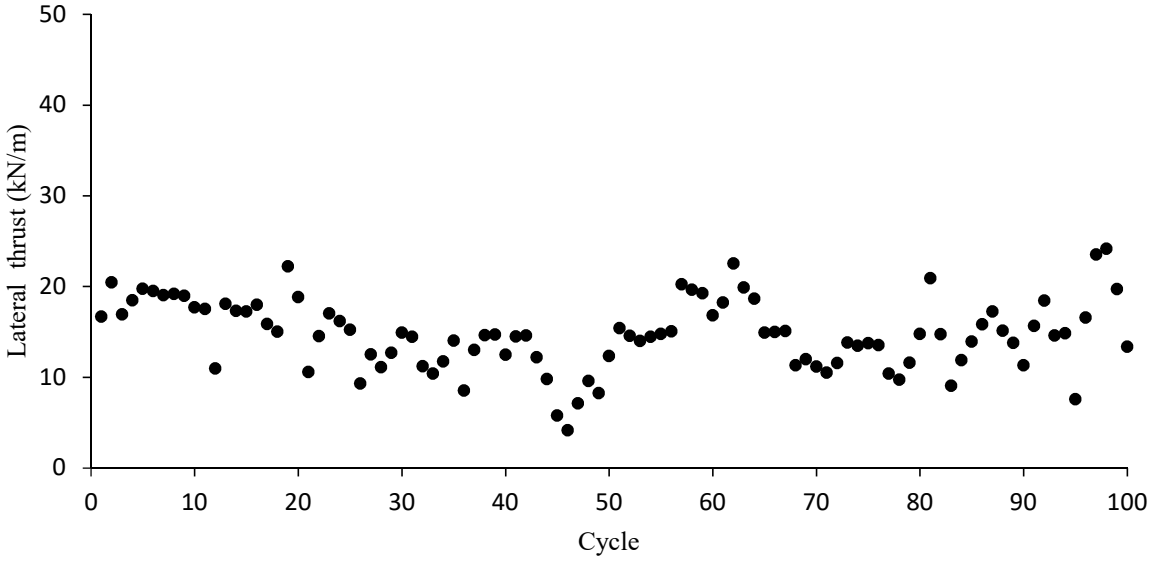

Figure 5. Passive lateral thrust on the abutment.

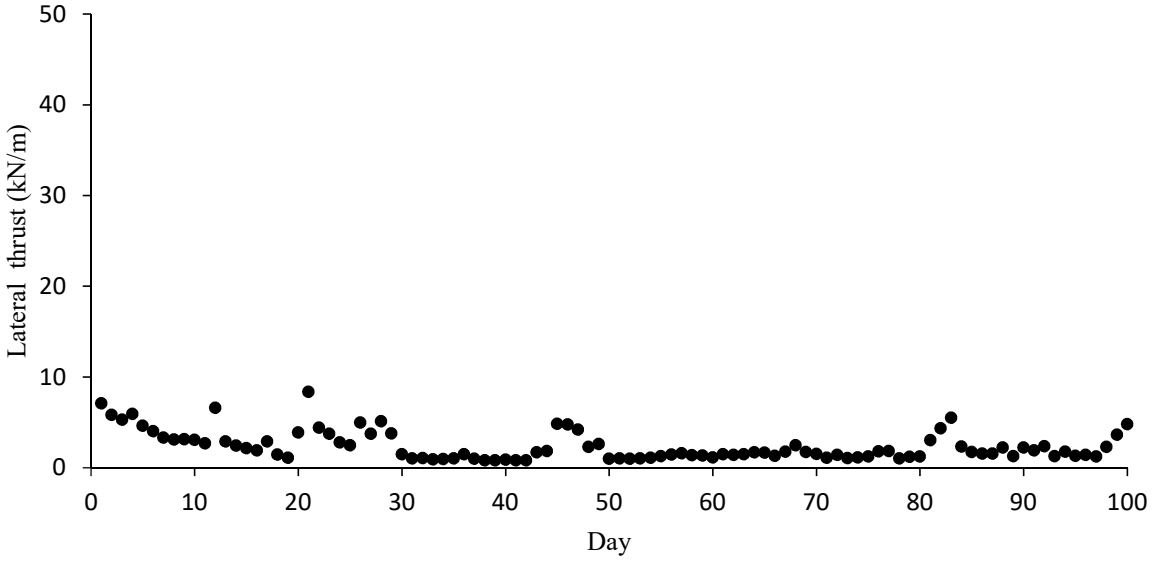

Figure 6. Active lateral thrust on the abutment.

The passive lateral thrust remained below 30 kN/m throughout the 100 cycles. Trends for the passive lateral thrust can be identified as the cycles go by. Firstly, the passive lateral thrust shows a tendency of reduction between the 1st and 46th cycles. Then, the passive lateral thrust increases until the 62nd cycle and decreases until the 71th cycle. The data becomes too disperse from the 71th cycle, so that a clear tendency cannot be recognized. The active lateral thrust remained below 10 kN/m during

the 100 cycles. The tendencies identified in the variations of the active lateral thrust are firstly characterized by a decrease within the first 19 cycles, with some scatter occurring between the 19th and 30th cycles. The active lateral thrust becomes constant after the 30th cycle. The active thrust appeared to be less affected by the cyclic oscillations of the lateral displacements of the bridge than the passive lateral thrust.

Figure 7 shows the vertical displacement of the soil surface along the distance from the abutment for selected cycles (20th, 40th, 60th, 80th and 100th cycles). The positive sign in the graph means downward vertical displacement (settlement) of the soil surface. Settlements increase with cycles and no tendency of stabilization within the 100 cycles was observed. The largest vertical displacement occurs at the backfill-abutment interface and gradually decreases with the distance from the abutment. The distance of influence can be assumed as 1 m and no upward vertical displacement (heave) of the soil surface was observed behind the abutment.

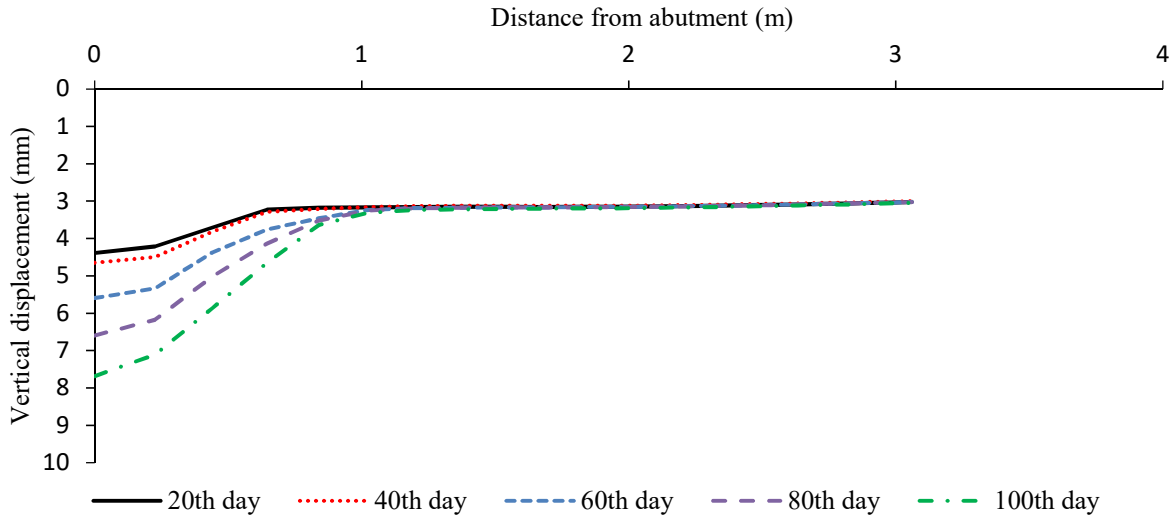

Figure 7. Vertical displacement of the surface of the soil behind the abutment.

After validation of the numerical model, numerical simulations were carried out with horizontal displacement amplitudes of ±5 mm and ±10 mm. The amplitude of ±5 mm was chosen based on AASHTO [28] and represents 0.5% of the abutment height. This value can be assumed as a serviceability limit. The amplitude of ±10 mm was chosen to represent a displacement of 1% of the abutment height and this value can be assumed as an ultimate limit. Bloodworth et al. [30] and Caristo et al. [16] performed numerical simulations of integral abutment bridges by applying 100 and 120 cycles, respectively, and found out that 30 cycles were enough for reaching the steady state in their investigated cases. Therefore, the numerical simulations were limited to 50 cycles due to the high computational cost.

Figure 8 and 9 show the evolution of the lateral thrust with the cycles for the chosen horizontal displacement amplitudes. The passive lateral thrust increased until around the 10th cycle and approached a nearly constant stable value, while the active lateral thrust remained virtually constant from the beginning. For contraction movements of the bridge, there seems to be no effect of the cycles on the lateral thrust. The escalation of the lateral thrust with larger displacements was also reported by England et al. [31] from results of small-scale tests of retaining wall models relating how the horizontal and vertical strains behave with amplitudes. Under high amplitudes of cycles, the soil mass near the backfill tends to compress laterally and expand vertically, which causes increase of the lateral thrust. Moreover, the steady state is reached after a few cycles.

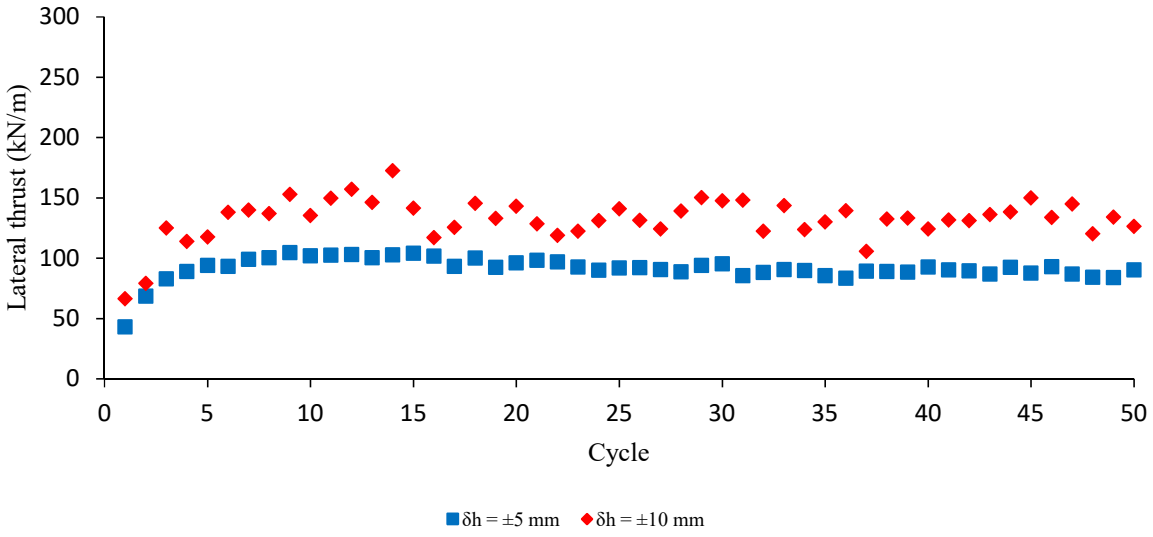

Figure 8. Passive lateral thrust under different cyclic displacement amplitudes.

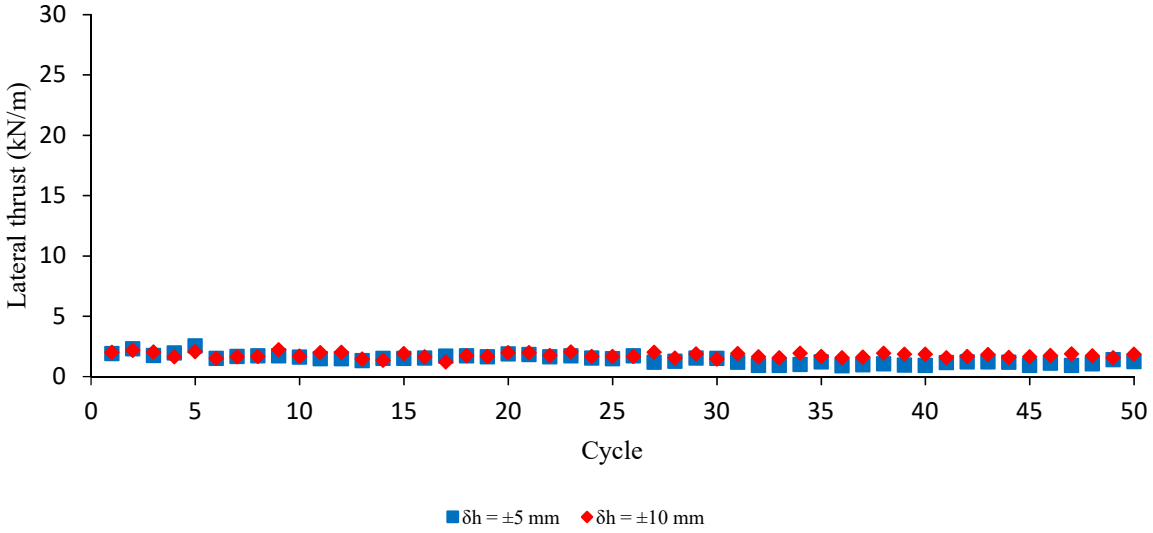

Figure 9. Active lateral thrust under different cyclic displacement amplitudes.

Profiles of vertical displacements of the soil surface behind the abutment are shown in Figures 10 and 11 for selected cycles (5^{th}, 10^{th}, 15^{th}, 20^{th} and 25^{th} cycles). The magnitude of the vertical displacements was found to increase with increasing cycles and amplitudes of imposed lateral displacements. The cyclic displacement provoked the appearance of a settlement region of the free-soil surface next to the abutment and a heave region of the free-soil surface at greater distances from the abutment. Settlements were maximum adjacent to the abutment and the heave of the free-soil surface indicates the existence of a flow mechanism within the backfill. The passive-active abutment movements produced a granular flow away from the abutment and the extension of the disturbance in the soil surface increased with increasing amplitude of displacements. Moreover, the vertical displacement progressively grew with increasing number of cycles in both amplitudes and there was no indication that a limiting value was being approached.

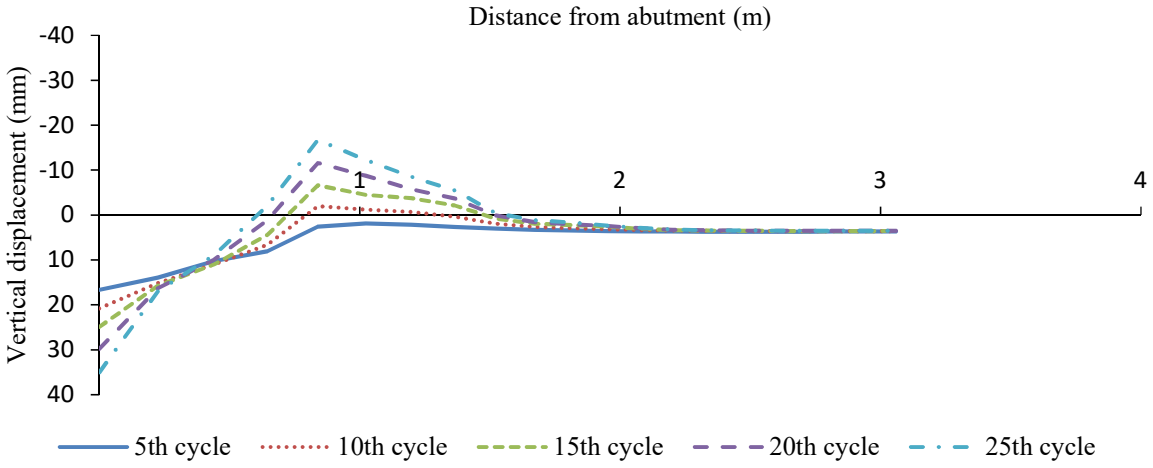

Figure 10. Profiles of vertical displacements on the surface of the backfill behind the bridge abutment, with a lateral displacement amplitude of ± 5 mm.

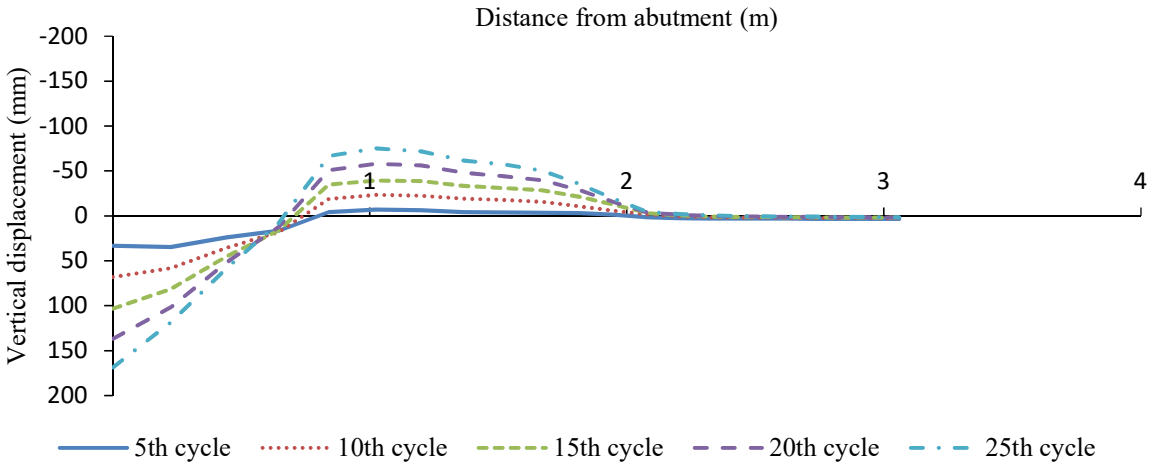

Figure 11. Profiles of vertical displacements on the surface of the backfill behind the bridge abutment, with a lateral displacement amplitude of ± 10 mm.

4 Concluding remarks

The present work presented the effects of cyclic lateral displacement amplitudes on lateral thrusts and settlements on a granular soil retained by a semi-integral abutment through numerical simulations. A numerical model was developed and calibrated from field data of an instrumented and monitored semi-integral abutment. The main findings of this work are as follows:

- The maximum thrust presented a variable behavior with the cycles, which included alternating reduction and escalation. The maximum thrust remained below Rankine's passive thrust. The minimum thrust, on the other hand, showed an initial reduction followed by stabilization with the cycles (steady state). The minimum thrust after stabilization remained around the Rankine's active thrust;
- Settlements progressed with abutment cyclic movements, without tendency of stabilization and heave of the soil surface, reaching an influence distance of about 1 m behind the abutment;
- Higher amplitudes of lateral displacements caused an increase of the passive lateral thrust

until around the 10th cycle and approached a nearly constant stable value, while the active lateral thrust remained virtually constant from the beginning;

- Settlements, heaves and the disturbance zone within the backfill soil behind the abutment increased with the lateral displacement amplitude, with maximum settlements next to the abutment and heave at greater distances from the abutment.

References

[1] I. Husain and D. Bagnariol. *Semi-integral abutment bridges*. Ministry of Transportation, Ontario, 1999.
[2] V. C. Mistry, 2005. Integral abutment and Jointless bridges. In: *The 2005 – FHWA Conference*, pp. 3–11.
[3] R. F. Maruri and S. H. Petro, 2005. Integral abutments and jointless bridges (IAJB) 2004 survey summary. In: *The 2005 – FHWA Conference*, pp. 12–29.
[4] C. W. W. Ng, S. M. Springman and A. R. M. Norrish. Centrifuge modeling of spread-base integral bridge abutments. *Journal of Geotechnical and Geoenvironmental Engineering*, vol. 124, n. 5, pp. 376-388, 1998.
[5] R. J. Lock. Integral bridge abutments. M. Eng. Project Report, University of Cambridge, 2002.
[6] S. A. Civjan, E. Kalayci, B. H. Quinn, S. F. Breña and C. A. Allen. Observed integral abutment bridge substructure response. *Engineering Structures*, vol. 56, pp. 1177-1191, 2013.
[7] A. J. Lutenegger, T. A. Thomson and C. Riccardi. Passive earth pressures in integral bridge abutments: progress report year 2. UMTC-97-19, University of Massachusetts, 1997.
[8] J. M. Franco. Design and field testing of jointless bridges. Master Thesis, West Virginia University, 1999.
[9] S. Breña, C. Bonczar, S. Civjan, J. DeJong and D. Crovo. Evaluation of seasonal and yearly behavior of an integral abutment bridge. *J Bridge Eng,* vol. 12, n. 3, pp. 296–305, 2007.
[10] S. Hasiotis and K. Xiong. Deformation of cohesionless fill due to cyclic loading: final report. SPRID#C-05-03, Stevens Institute of Technology, 2007.
[11] F. Tatsouka, D. Hirakawa, M. Nojiri, H. Aizawa, H. Nishikiori, R. Soma, M. Tateyama and K. Watanabe. A new type of integral bridge comprising geosynthetic-reinforced soil walls. *Geosynthetics International*, vol. 16, n. 4, pp. 301-326, 2009.
[12] H. Munoz, F. Tatsouka, D. Hirakawa, H. Nishikiori, R. Soma, M. Tateyama and K. Watanabe. Dynamic stability of geosynthetic-reinforced soil integral bridge. *Geosynthetics International*, vol. 19, n. 1, pp. 11-38, 2012.
[13] S. Argyroudis, A. Palaiochorinou, S. Mitoulis and D. Pitilakis. Use of rubberised backfills for improving the seismic response of integral abutment bridges. *Bull Earthquake Eng*, vol. 14, pp. 3573-3590, 2016.
[14] M. Saghebfar, M. Abu-Farsakh, A. Ardah, Q. Chen and B. A. Fernandez. Performance monitoring of geosynthetic reinforced soil integrated bridge system (GRS-IBS) in Louisiana. *Geotextiles and Geomembranes*, vol. 45, pp. 34-47, 2017.
[15] S. A. Huntley and A. J. Valsangkar. Behavior of H-piles supporting an integral abutment bridge. *Can. Geotech. J.*, vol. 51, pp. 713-734, 2013.
[16] A. Caristo, J. Barnes and S. A. Mitoulis. Numerical modelling of integral abutment bridges under seasonal thermal cycles. *Proceedings of the Institution of Civil Engineers – Bridge Engineering*, vol. 171, n. 3, pp. 179-190, 2018.
[17] J. R. Walter. Experimental and numerical investigation of integral/semi-integral bridge abutments for Texas conditions. Master Thesis, The University of Texas, 2018.
[18] J.A. Knappett, K. Caucis, M. J. Brown, J. R. Jeffrey and J. D. Ball. CHD pile performance: part II – numerical modelling. *Proceedings of the Institution of Civil Engineers – Geotechnical Engineering*, vol. 169, n. 5, pp. 436–454, 2016.
[19] S. Rawat and A. S. Gupta. Numerical modelling of pullout of helical soil nail. *Journal of Rock Mechanics and Geotechnical Engineering*, vol. 9, n. 4, pp. 648–658, 2017.
[20] S. Khanal. Backcalculation of plate loading tests using Plaxis 2D and the hardening soil model. Master Thesis, Norwegian University of Science and Technology, 2013.

[21] H. G. Poulos and E. H. Davies. *Elastic solutions for soil and rock mechanics*. John Williams & Sons, 1974.
[22] M. A. Stroud and F. G. Butler, 1975. The standard penetration test and the engineering properties of glacial materials. In: Symp. on Engineering Properties of Glacial Materials, pp.117-128.
[23] G. Mesri. New design procedure for stability of soft clays. *J. Geotech. Eng. Div.,* vol. 101, pp. 409-412, 1975.
[24] F. H. Kulhawy and P. W. Mayne. Manual on estimating soil properties for foundation design. Final Report, Cornell University, 1982.
[25] M. J. Tomlinson. *Pile design and construction practice*. E & FN Spon, 1993.
[26] M. Karalar and M. Dicleli. Fatigue in jointless bridge H-piles under axial load and thermal movements. *Journal of Constructional Steel Research*, vol. 147, pp. 504-522, 2018.
[27] B. Murphy and M. Yarnold. Temperature-driven structural identification of a steel girder bridge with an integral abutment. *Engineering Structures*, vol. 115, pp. 209-221, 2018.
[28] AASHTO. *LRFD bridge: design specifications*. 2012.
[29] L. E. Rodriguez, P. J. Barr and M. W. Halling. Temperature effects on a box-girder integral-abutment bridge. *Journal of Performance of Constructed Facilities*, vol. 28, n. 3, pp. 583-591, 2014.
[30] A. G. Bloodworth, M. Xu, J. R. Banks and C. R. I. Clayton. Predicting the earth pressure on integral bridge abutments. *Journal of Bridge Engineering*, vol. 17, n. 2, pp. 371-381, 2012.
[31] G. L. England, N. C. M. Tsang and D. I. Bush. *Integral bridges: a fundamental approach to the time-temperature loading problem*. Thomas Telford, 2000.